Strain gradient effects on steady state crack growth in rate-sensitive materials

K.L. Nielsen [a,*], C.F. Niordson [a], J.W. Hutchinson [b]

[a] Department of Mechanical Engineering, Solid Mechanics, Technical University of Denmark, DK-2800 Kgs. Lyngby, Denmark
[b] School of Engineering and Applied Sciences, Harvard University, 29 Oxford Street, Cambridge, MA 02138, USA

ARTICLE INFO

ABSTRACT

Steady state crack propagation produce substantial plastic strain gradients near the tip, which are accompanied by a high density of geometrically necessary dislocations and additional local strain hardening. Here, the objective is to study these gradient effects on Mode I toughness of a homogeneous rate-sensitive metal, using a higher order plasticity theory. Throughout, emphasis is on the toughness rate-sensitivity, as a recent numerical study of a conventional material (no gradient effects) has indicated a significant influence of both strain rate hardening and crack tip velocity. Moreover, a characteristic velocity, at which the toughness becomes independent of the rate-sensitivity, has been observed. It is the aim to bring forward a similar characteristic velocity for the current strain gradient visco-plastic model, as-well as to signify its use in future visco-plastic material modeling.

© 2012 Elsevier Ltd. All rights reserved.

1. Introduction

The fracture toughness of elastic–plastic materials is primarily governed by plastic dissipation that decomposes into irrecoverable heat energy and cold work associated with the dislocation structure [1–9], which in turn is responsible for the phenomenon of stable crack growth [1,10,11]. At steady state crack advance, under small-scale yielding, the remote elastic region follows the classical solution with a $\sqrt{r}$-singularity in the stress field, while an active plastic zone travels with the crack tip and shields it from the surrounding elastic stress–strain fields. Trailing behind, is a residual plastic strain wake where elastic unloading takes place, and where a secondary loading zone exists in terms of reverse plastic deformation so that the material remains in yielding close to the free fracture surface. The size and shape of these plastic regions, and thus the macroscopic material toughness, are controlled by a wide range of parameters, characterizing material properties and loading conditions. This has been extensively studied in the literature using both steady state [1,2,4,5,11,12], and Lagrangian [6–8,13] model formulations. It is well known that properties such as the strain hardening, and thereby the evolution of the local flow stress, significantly influences on the dissipated energy, thus on the energy needed to advance the crack in the presence of plasticity. Any hardening effect, such as additional hardening owing to strain gradients should therefore be expected to play a noticeable role on the macroscopic fracture toughness.

To model experimentally observed gradient effects [14–17], a range of so-called higher order theories have been developed, counting both phenomenological [18–22], and micro-mechanics based [23–26] models. Moreover, a great deal of effort has gone into applying the various models to interface cracking under stationary conditions [5,27–31]. Using the modeling procedure by [1], developed for steady state structural analysis, Wei and Hutchinson [27] analyzed Mode I crack growth in homogeneous rate-independent metals with focus on gradient effects. Special attention was given to the tractions acting on

* Corresponding author. Tel.: +45 4525 4258; fax: +45 4593 1475.
  E-mail address: kin@mek.dtu.dk (K.L. Nielsen).

Nomenclature

$\dot{a}$	crack tip velocity
D	SSV parameter
E, G, v	Young's modulus, Shear modulus and Poisson ratio, respectively
$E^p, \dot{E}^p$	effective plastic strain and plastic strain rate, respectively
$f_{ij}(\theta)$	dimensionless mode functions
$J_{\text{tip}}, J_{\text{ss}}$	energy release rate at crack tip and at steady state, respectively
K_I	stress intensity factor
L_D, L_E	dissipative and energetic length parameter, respectively
τ_{ijk}	total higher order stress tensor
$\tau_{ijk}^D, \tau_{ijk}^E$	dissipative and energetic part of the higher order stress tensor, respectively
M_{ij}	higher order tractions
N, m	strain hardening and strain rate hardening, respectively
q_{ij}	micro-stress tensor
q_{ij}^D, q_{ij}^E	dissipative and energetic part of micro-stress tensor, respectively
r	radial distance from crack tip
R_0, R_{ss}	reference plastic zone size and steady state plastic zone size, respectively
s_{ij}	Cauchy stress deviator
T_i	conventional traction vector
u_i	displacement field
x_k	Cartesian coordinates
$\mathcal{L}_{ijkl}$	isotropic elastic stiffness tensor
σ_{ij}	Cauchy stress tensor.
σ_y, σ_e	initial yield stress and von Mises stress, respectively
σ_c	gradient enhanced effective stress
$\dot{\varepsilon}_0$	reference strain rate
$\varepsilon_{ij}, \varepsilon_{ij}^e, \varepsilon_{ij}^p$	total strain, elastic strain and plastic strain tensor, respectively
$\varepsilon_{ij,k}^p, \dot{\varepsilon}_{ij,k}^p$	gradient of plastic strain and plastic strain rate, respectively
θ	relaxation parameter
Ψ	free energy
Γ_{tip}	fracture energy release at the crack tip

the plane ahead of the crack tip (see also [28]), the crack opening displacement, the shape of the active plastic zone, and the associated change in the macroscopic fracture toughness, based on a cohesive zone modeling approach for the near tip fracture process. Their work was later continued in [5] for interface failure, where the model by Suo et al. [3] (SSV-model) is reviewed and unified with a cohesive zone model. While the above studies are carried out using the phenomenological gradient enhanced J_2-flow theory by Fleck and Hutchinson [18], similar studies for rate-independent mechanism-based strain gradient (MSG) theories can be found in the literature. Jiang et al. [29], conducted an analysis of the stress field surrounding the crack tip, in order to provide a means to explain cleavage cracking in metals. Wei et al. [31], compared their steady state Mode I crack analysis, using an MSG theory by Qiu et al. [26], to predictions in [27]. Similar trends were obtained using MSG theory, but with a length parameter 4–5 times the corresponding quantity in the Fleck-Hutchinson theory.

The objective of this study is to analyze steady state Mode I fracture in elastic-viscoplastic strain gradient enhanced metallic materials, and thereby to bring out the combined effects of rate-sensitivity and strain gradient hardening on the macroscopic fracture toughness. The viscous behavior of metals undergoing deformation, e.g. at elevated temperatures, is known to be an important factor concerning plastic dissipation, and the assumption of a rate-independent response is typically not easily justified. In a recent study, Nielsen and Niordson [9], demonstrated this, using a conventional elastic-viscoplastic material model without gradient effects. When compared to the rate-independent toughness, a significant increase in fracture toughness exists for slowly growing cracks, while a decrease was found for fast growing cracks. Moreover, this study revealed a characteristic velocity at which the fracture toughness becomes independent of the material strain rate hardening, and thus equal to the rate-independent toughness. This was argued based on the time aspect of the stress build-up/relaxation in the vicinity of the crack tip, but unfortunately no physical interpretation can be made of this velocity. Furthermore, the predicted characteristic velocity is yet to be identified in experiments. The finding of this characteristic velocity fertilizes multiple questions regarding future modeling of viscoplastic materials. E.g. *does a similar characteristic velocity exist for other and more advanced constitutive models? Does the characteristic velocity allow for extracting information on the rate-independent toughness which can be difficult to assess directly?* In the present study, we consider a gradient enhanced material model by Gudmundson [20] , (see also [21,32]), which is based on a similar visco-plastic framework as the conventional model used in [9]. However, the current model formulation differs substantially from the conventional model, but

approaches its response in case of small strain gradients, or equivalently by letting the length parameter go to zero. Moreover, equivalent to the conventional model, the gradient enhanced model is rather cumbersome in terms of stability, when approaching the rate-independent limit for which the theory is incomplete at present. This model is therefore ideally used to shed light on the questions raised above.

The paper is structured as follows. The classical boundary value problem of a semi-infinite crack, advancing at steady state under Mode I loading is briefly summarized in Section 2, while the material model formulation and numerical procedure are presented in Section 3. Attention is given to the steady state procedure, which has been adapted for integration of the current gradient enhanced elastic-viscoplastic material model. The results of the analysis are laid out in Section 4, where the combined effect of material rate-sensitivity and strain gradient hardening are illustrated. Moreover, Section 4 presents a method that allows for extracting the rate-independent toughness without approaching this limit numerically. Some concluding remarks are given in Section 5.

2. Problem formulation

Fig. 1 illustrates the Mode I crack growth problem considered in the present study. The crack is assumed to grow under stationary conditions, with constant velocity, $\dot{a}$, so that the near tip stress and strain fields are fully developed. To link the macroscopic and the microscopic scales, and thereby to model the shielding ratio, J_{ss}/J_{tip}, a variation of the SSV-model by Suo et al. [3] is adopted in this study (see Section 3). Plane strain conditions and small scale yielding are assumed, while the effect of material inertia is neglected. Remote Mode I loading is applied on the outer boundary according to the elastic solution of a semi-infinite interface crack [33], whereby the remote stress field is given in terms of the remote K_I stress intensity factor

$$\sigma_{ij} = \frac{K_I}{\sqrt{2\pi r}} f_{ij}(\theta). \tag{1}$$

Here, θ is the angle from the positive x_1-direction, r is the distance from the crack tip and $f_{ij}(\theta)$ are the dimensionless mode functions. By defining the length quantity, R_0, as the reference plastic zone size

$$R_0 = \frac{1}{3\pi} \left(\frac{K_I}{\sigma_y}\right)^2, \quad \text{and} \quad K_I = \sqrt{\frac{E\Gamma_{tip}}{1 - v^2}}. \tag{2}$$
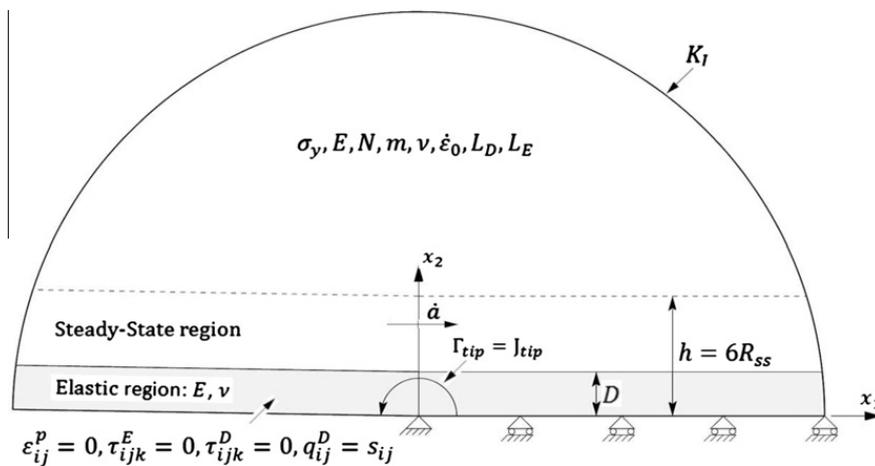
Fig. 1. Stationary Mode I crack growth in rate-sensitive materials, subject to a remote elastic K_I-field. Employing the SSV model, an elastic material strip of total width "D" is introduced around the crack, and the elastic material properties (E and v) are kept constant throughout the material. Symmetry is enforced in the displacement field along $x_1 \geqslant 0$ at $x_2 = 0$, while a discussion on the higher order boundary conditions can be found in Section 3.3.

Table 1
Mechanical properties.

Parameter	Significance	Value
E	Youngs modulus	200 GPa
v	Poisson's ratio	0.3
σ_y	Initial yield stress	200–600 MPa
N	Strain hardening exponent	0.1–0.5
m	Strain rate hardening exponent	0.01–0.1
$\dot{\varepsilon}_0$	Reference strain rate	0.002 s^{-1}
Γ_{tip}	Near tip fracture energy	1 J/m^2
L_D/R_0	Dissipative length parameter	0–0.8
L_E/R_0	Energetic length parameter	0

the fracture energy release rate at the crack tip, Γ_{tip}, enters as a near tip fracture criterion through the linear elastic fracture criterion ($J_{\text{tip}} = \Gamma_{\text{tip}}$), which applies in the elastic strip introduced by Suo et al. [3] (see Section 3). Here, Γ_{tip} denotes the microscopic fracture energy, while E is Young's modulus, v is Poisson ratio and σ_y is the initial yield stress (see Table 1). The macroscopic toughness at steady state, J_{ss}, is in the following related to the corresponding K_{ss}-field, prescribed to the outer boundary, through an expression similar to Eq. (2).

3. Model: constitutive relation and numerical procedure

3.1. Rate-sensitive constitutive model

The crack growth problem is analyzed using a gradient enhanced elastic-viscoplastic material model proposed by [20,21,32]. Employing a small strain formulation, an additive decomposition of the total strain is applied, so that $\varepsilon_{ij} = \varepsilon_{ij}^e + \varepsilon_{ij}^p$, where ε_{ij}^e is the elastic part and ε_{ij}^p is the plastic part. The total strain field is determined from the displacements, which together with the plastic strain components are determined based on the principle of virtual work for the current higher order material. In Cartesian components, this writes

$$\int_V \left(\sigma_{ij}\delta\varepsilon_{ij} + (q_{ij} - s_{ij})\delta\varepsilon_{ij}^p + \tau_{ijk}\delta\varepsilon_{ij,k}^p \right) dV = \int_S \left(T_i\delta u_i + M_{ij}\delta\varepsilon_{ij}^p \right) dS. \tag{3}$$

Here, q_{ij} is the micro-stress tensor, $s_{ij} = \sigma_{ij} - \delta_{ij}\sigma_{kk}/3$ is the Cauchy stress deviator and τ_{ijk} is the higher order stresses, work conjugate to the plastic strain gradients, $\varepsilon_{ij,k}^p$. Here, $(\ )_{,k}$ denotes the partial derivative with respect to the coordinate x_k. The right hand side of the principle of virtual work includes the conventional traction vector $T_i = \sigma_{ij}n_j$, work conjugate to the displacements, and the higher order tractions $M_{ij} = \tau_{ijk}n_k$, work conjugate to the plastic strains.

Usually, plastic deformation is mainly considered to be a dissipative process that covers irrecoverable heat energy and cold work, whereby no free energy is associated with the plastic strain itself. At large length scales, corresponding to the conventional limit (small strain gradients), all energy associated with plastic deformation should therefore be dissipated. However, when large plastic strain gradients appear, geometrically necessary dislocations (GNDs) are stored [34], which gives rise to free energy associated with the local stress field of the GNDs [24,35], as-well as increased dissipation when the GNDs move in the lattice. These mechanisms were originally incorporated into this higher order material model by assuming the micro-stress to have a dissipative part, $q_{ij} = q_{ij}^D$, only, while the higher order stresses decompose into a dissipative part, τ_{ijk}^D, and an energetic part, τ_{ijk}^E, so that: $\tau_{ijk} = \tau_{ijk}^D + \tau_{ijk}^E$. Thus, the free energy can be introduced according to the isotropic expression

$$\Psi = \frac{1}{2}\left(\varepsilon_{ij} - \varepsilon_{ij}^p\right)\mathcal{L}_{ijkl}(\varepsilon_{kl} - \varepsilon_{kl}^p) + \frac{1}{2}G(L_E)^2\varepsilon_{ij,k}^p\varepsilon_{ij,k}^p \tag{4}$$

whereby the conventional stresses is given through the elastic relationship: $\sigma_{ij} = \mathcal{L}_{ijkl}\left(\varepsilon_{kl} - \varepsilon_{kl}^p\right)$, while the energetic higher order stresses are: $\tau_{ijk}^E = G(L_E)^2\varepsilon_{ij,k}^p$. Here, $\mathcal{L}_{ijkl}$ is the isotropic elastic stiffness tensor, G is the elastic shear modulus and L_E is the isotropic energetic constitutive length parameter. In this study, the energetic length parameter is taken to be zero throughout.

The corresponding dissipative quantities are derived from a visco-plastic potential, consistent with [20] and [32], where the effective stress, $\sigma_c = \sigma_c(\dot{E}^p, E^p)$, is taken to depend both on the accumulated effective plastic strain, E^p, and the current gradient enhanced effective strain rate

$$\dot{E}^p = \sqrt{\frac{2}{3}\dot{\varepsilon}_{ij}^p\dot{\varepsilon}_{ij}^p + (L_D)^2\dot{\varepsilon}_{ij,k}^p\dot{\varepsilon}_{ij,k}^p}. \tag{5}$$

Here, L_D is the dissipative length parameter, and $\dot{\varepsilon}_{ij,k}^p$ are the rates of the plastic strain gradients. The length parameter L_D is included for dimensional consistency. It scales the dissipation contribution from geometrically necessary dislocations to that arising from plastic deformation in the absence of plastic strain gradients. Following [20], the dissipative stresses are given by

$$q_{ij}^D = \frac{2}{3}\frac{\sigma_C[\dot{E}^p, E^p]}{\dot{E}^p}\dot{\varepsilon}_{ij}^p, \qquad \text{and} \qquad \tau_{ijk}^D = \frac{\sigma_C[\dot{E}^p, E^p]}{\dot{E}^p}(L_D)^2\dot{\varepsilon}_{ij,k}^p \tag{6}$$

while the associated effective stress measure is

$$\sigma_C = \sqrt{\frac{3}{2}q_{ij}^D q_{ij}^D + (L_D)^{-2}\tau_{ijk}^D \tau_{ijk}^D} \tag{7}$$

A power-law relation for the visco-plastic behavior is assumed, so that

$$\dot{E}^p = \dot{\varepsilon}_0\left(\frac{\sigma_C}{g(E^p)}\right)^{1/m}, \qquad \text{with} \qquad g(E^p) = \sigma_y\left(1 + \frac{EE^p}{\sigma_y}\right)^N \tag{8}$$

where N is the power hardening exponent, m is the strain rate hardening exponent and $\dot{\varepsilon}_0$ is the reference strain rate. In this model, the visco-plastic behavior becomes significant for high values of the strain rate hardening exponent, m, while the cur-

rent constitutive material model approaches the response of a J_2-flow material model in the rate-independent limit ($m \rightarrow 0$). Moreover, the response of the gradient enhanced model reduces to the prediction of its corresponding conventional version for zero length scales ($L_E = L_D = 0$).

3.2. Steady state formulation and numerical procedure

In this study, a steady state finite element (FE) formulation is chosen over a classical transient FE model since it directly brings out the crack tip field under stationary conditions, which is the aim for this analysis. Thus, the convergence of any transient behavior is avoided, which in turn makes the steady state formulation much faster in terms of calculation time. Dean and Hutchinson [1], define steady state as the condition at which the stress field and strain field surrounding the advancing crack tip remains unchanged to an observer moving with the tip. Thus, any time derived quantity, $\dot{f}$, in the constitutive model can be related to the spatial derivative through the crack velocity, $\dot{a}$, along the x_1-direction, according to

$$\dot{f} = -\dot{a}\frac{\partial f}{\partial x_1}. \tag{9}$$

An incremental quantity, in a given material point (x_1^*, x_2^*), can then be evaluated by a streamline integration along the negative x_1-direction, which starts well in front of the active plastic zone (upstream, $x_1 = x_0 \gg 0$, $x_2 = x_2^*$) and ends at the point of interest $(x_1 = x_1^*, x_2 = x_2^*)$. This spatial streamline integration is carried out using a standard forward Euler time integration, with the point of interest holding the history of all upstream material points.

For the adopted model formulation, the conventional principle of virtual work for quasi-static problems can be use to determine the displacement field, u_i,

$$\int_V \delta\varepsilon_{ij}\mathcal{L}_{ijkl}\varepsilon_{kl}dV = \int_S \delta u_i T_i dS + \int_V \delta\varepsilon_{ij}\mathcal{L}_{ijkl}\varepsilon_{kl}^p dV \tag{10}$$

whereas a corresponding Minimum Principle can be formulated for the plastic strain rate field [32],

$$\int_V \left(q_{ij}^D \delta\dot{\varepsilon}_{ij}^p + \tau_{ijk}^D \delta\dot{\varepsilon}_{ij,k}^p\right)dV = \int_V \left(s_{ij}\delta\dot{\varepsilon}_{ij}^p - \tau_{ijk}^E \delta\dot{\varepsilon}_{ij,k}^p\right)dV + \int_S M_{ij}\delta\dot{\varepsilon}_{ij}^p dS. \tag{11}$$

The displacement field, and the related plastic strain rate field thereby decouple partially, whereby a solution can be iterated upon in a "staggered" approach, with one solution limping behind the other.

The numerical implementation of the current visco-plastic strain gradient enhanced model follows that of [36]. Thus, based on the Minimum Principles in Eqs. (10) and (11), a standard finite element interpolation of the form

$$\dot{u}_i = \sum_{n=1}^{8} N^{(n)}\dot{u}_i^{(n)} \quad \text{and} \quad \dot{\varepsilon}_{ij}^p = \sum_{n=1}^{4} N^{(n)}\dot{\varepsilon}_{ij}^{(n)} \tag{12}$$

can be introduced for the displacement increments and the plastic strain rate field, respectively. Here, 8-node isoparametric plane strain elements are used for the discretization of the displacement field, and corresponding 4-node elements are used for the plastic strain rate field. Both element types are integrated using Gauss quadrature, with 2×2 Gauss points. The nodal solution is iterated upon following a steady state integration procedure similar to that of [1,9,12,27]. Here, the corresponding gradients to the nodal fields are readily derived in line with the standard displacement-to-strain matrix based on Eq. (12). The basis of this numerical procedure is summarized below.

(1) Based on the plastic strains from the earlier iteration, $\varepsilon_{ij}^{p(n-1)}$, the current displacement field, $u_i^{(n)}$, is determined from Eq. (10).
(2) Compute the total strain, $\varepsilon_{ij}^{(n)}$, from the current displacement field, $u_i^{(n)}$.
(3) Determine the plastic strain rate field, $\dot{\varepsilon}_{ij}^{p(n)}$, iteratively:
   do m = 1, . . .
   (A) Determine $\dot{\varepsilon}_{ij}^{p(m)}$ from Eq. (11), based on $\dot{\varepsilon}_{ij}^{p*(m-1)}$ and evaluate

$$\dot{\varepsilon}_{ij}^{p*(m)} = (1-\theta)\dot{\varepsilon}_{ij}^{p*(m-1)} + \theta\dot{\varepsilon}_{ij}^{p(m)} \tag{13}$$

with θ being a relaxation parameter introduced to enhance stability.
   (B) Update $\dot{\varepsilon}_{ij,k}^{p(m)}$, $\dot{E}^{p(m)}$, $q_{ij}^{D(m)}$ and $\tau_{ijk}^{D(m)}$, based on $\dot{\varepsilon}_{ij}^{p*(m)}$.
   (C) Perform streamline integration ($\varepsilon_{ij}^{p(m)} = 0$ outside steady-state region)

$$\varepsilon_{ij}^{p(m)} = \int_{x_0}^{x^*} \frac{\partial\varepsilon_{ij}^{p(m)}}{\partial x_1}dx_1, \qquad \text{with} \qquad \frac{\partial\varepsilon_{ij}^{p(m)}}{\partial x_1} = -\frac{1}{\dot{a}}\dot{\varepsilon}_{ij}^{p*(m)} \tag{14}$$

$$\varepsilon_{ij,k}^{p(m)} = \int_{x_0}^{x^*} \frac{\partial\varepsilon_{ij,k}^{p(m)}}{\partial x_1}dx_1, \qquad \text{with} \qquad \frac{\partial\varepsilon_{ij,k}^{p(m)}}{\partial x_1} = -\frac{1}{\dot{a}}\dot{\varepsilon}_{ij,k}^{p*(m)} \tag{15}$$

$$E^{p(m)} = \int_{x_0}^{x^*} \frac{E^{p(m)}}{\partial x_1}dx_1, \qquad \text{with} \qquad \frac{E^{p(m)}}{\partial x_1} = -\frac{1}{\dot{a}}\dot{E}^{p(m)} \tag{16}$$

(D) Compute the current stress field, $\sigma_{ij}^{(m)}$, using the elastic relationship.

(E) Repeat steps A through D until convergence in $\dot{\varepsilon}_{ij}^{p*(m)}$ is achieved.

end do

(4) Repeat steps 1–3 until convergence is achieved. Convergence in both the displacement field and the stress field is here considered.

3.3. A variation of the SSV model

Suo et al. [3] put forward the SSV-model as a means of investigating cleavage cracking in the presence of plastic flow. Their model relies on the basic assumption that an elastic region, on the order of the dislocation spacing, surrounds the crack tip whereby the dislocations emitted at the tip play a minor role in the fracture process, and are unlikely to blunt the major portion of the crack front. In the steady state formulation, this implies that the crack lies fully within an elastic region of width 2D, whereby linear fracture mechanics applies and an elastic singularity exists near the tip (see Fig. 1). Thus, the elastic energy release rate is easily evaluated using the J-integral, whereby the criterion for crack propagation is: $J_{\text{tip}} = \Gamma_{\text{tip}}$, with Γ_{tip} being the work of separation which must be supplied by the local elastic crack tip field for crack advance to occur (see e.g. [5] for further details). For the case of plastic flow in regions bordering on the elastic SSV-strip of material, a large amount of the energy supplied to the far boundary goes into plastic deformation, whereas only parts of it reaches the crack tip. Thus, let J_{ss} be the steady state energy release rate supplied far from the tip, the ratio J_{ss}/J_{tip} quantifies the fraction of energy going into plastic deformation during crack growth.

It is recognized that substantial plastic strain gradients occur near the crack tip, which are accompanied by additional hardening associated with a high density of geometrically necessary dislocations (GNDs). Thus, in order to accurately estimate the stresses and the plastic dissipation during crack advance, a higher order continuum model is adopted in the present work. Additional boundary conditions most thereby be enforced, making this variation of the SSV model differ from that originally proposed by Suo et al. [3].

Using the current model set-up for Mode I cracking, dimensional analysis dictates that the crack tip shielding ratio at steady state is controlled by [5,37]

$$\frac{J_{ss}}{J_{\text{tip}}} = F\left(\frac{\dot{a}}{R_0\dot{\varepsilon}_0}, \frac{R_0}{D}, \frac{L_D}{R_0}, \frac{L_E}{R_0}, \frac{\sigma_y}{E}, N, m, \nu\right) \tag{17}$$

Moreover, the crack tip shielding ratio, J_{ss}/J_{tip}, is influenced by the choice of higher order boundary conditions, which by no means is trivial as the elastic region introduced by Suo et al. [3] is non-conventional. The "traditional" higher order boundary conditions with zero plastic strain rate at an elastic–plastic interface might therefore not be the obvious choice. Two sets of boundary conditions are considered: (i) constraint plastic flow at the elastic–plastic interface so that $\dot{\varepsilon}_{ij}^p = 0$ in the elastic strip ($x_2 \leqslant D$), and (ii) leaving the higher order tractions zero at the interface so that $M_{ij} = 0$ at $x_2 = D$ (enforced by neglecting the higher order stiffness in the elastic strip). Fig. 2 compares the predicted crack tip shielding ratio that reflects the macroscopic toughness owing to plasticity, as function of the SSV quantity R_0/D for the two sets of higher order boundary conditions. The comparison is made for both a slowly growing crack and a fast growing crack, with $L_D/R_0 = [0, 0.2]$. The figure shows that the predicted trends, using the two sets of boundary conditions, are comparable, although it is clear that a constraint on the plastic flow at the elastic–plastic interface ($\dot{\varepsilon}_{ij}^p = 0$ at $|x_2| \leqslant 0$) lowers the shielding ratio, especially when intro-
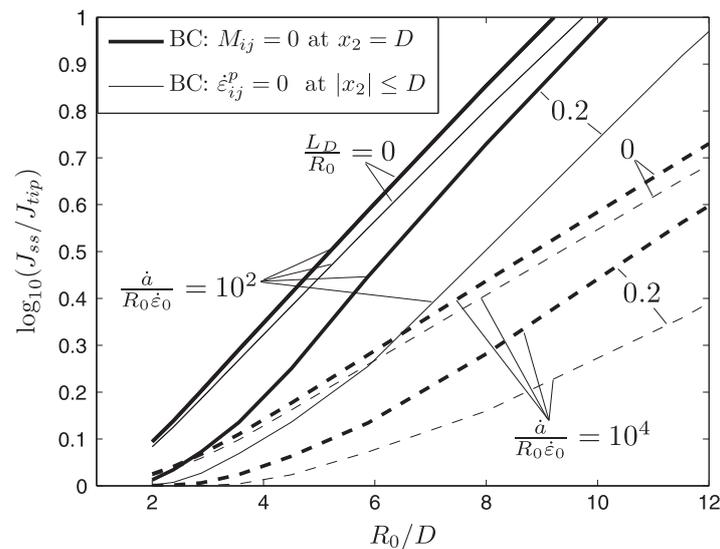
Fig. 2. Steady state fracture toughness vs. inverse elastic layer thickness (SSV parameter "D") emphasising the effect of the higher order boundary conditions. Here, results are shown for $N = 0.2$, $m = 0.05$, $L_D/R_0 = [0, 0.2]$, and $\dot{a}/(R_0\dot{\varepsilon}_0) = [10^2, 10^4]$.

ducing the dissipative length scale ($L_D \neq 0$). This has to do with the boundary layer of low plastic straining forming at the interface close to the crack tip, where substantial plastic strains and plastic strain gradients would otherwise occur. On the other hand, leaving the higher order stresses zero at the interface ($M_{ij} = 0$ at $x_2 = D$) eliminates this boundary layer, which in turn makes this model prediction comparable to a conventional (local) model when $L_D \to 0$. The second higher order boundary condtion is therefore adopted in the remaining part of this paper enabling a direct comparison with earlier published results by Nielsen and Niordson [9].

Throughout this work, the phrase "a slowly" or "a fast" growing crack refers to the velocity interval investigated as it spans four orders of magnitude, for which inertia effects can be neglected as the maximum velocity considered is $\dot{a} = 10^4 \cdot R_0\dot{\epsilon}_0$, with $R_0 \approx 0.1$–1 μm for materials failing by atomic separation (see [5]).

4. Results

Using a conventional model formulation, [9] recently showed that the macroscopic toughness of visco-plastic metals increases monotonically with increasing rate-sensitivity at low crack tip velocity, while it decreases monotonically with increasing rate-sensitivity at high crack tip velocity (independent of the strain hardening). This has to do with the stress build-up/relaxation, which is to be further elaborated on in the following (see also [9]). In the present work, predictions comparable to those of a conventional plasticity model are obtained for the current strain gradient enhanced model (see Fig. 3). In fact, by omitting the length scale effects ($L_D = 0$), the model predictions closely coincides, with negligible differences that are related to convergence issues.

Fig. 3 shows the predicted crack tip shielding ratio as function of the SSV quantity R_0/D for a slowly growing crack (in Fig. 3a) and a fast growing crack (in Fig. 3b) under Mode I loading. To bring out the combined effect of material rate-sensitivity and strain gradient hardening, results are shown for various strain rate hardening values ($m = [0.01, 0.05, 0.1]$), and dissipative length parameters ($L_D = [0, 0.2]$ for all cases, and $L_D \in [0, 0.8]$ for selected model settings). From Fig. 3, it is seen that the macroscopic toughness increases monotonically with increasing rate-sensitivity at low crack tip velocity, while it decreases monotonically with increasing rate-sensitivity at high crack tip velocity (see [9] for further discussion). In addition it is seen that an increase in length parameter, L_D, lowers the macroscopic fracture toughness. This is ascribed to additional hardening effects in the crack tip region, where the material undergoes substantial plastic deformation, which in turn leads to elevated stresses near the tip that enable satisfying the fracture criterion at much lower macroscopic loads. This hardening effect is also reflected in the von Mises stress field depicted in Fig. 4a as the variation along the streamline closest to the elastic strip ($x_2 \approx D$, thus near the SSV region). By accounting for the strain gradient hardening, the peak reference stress near the crack tip increases significantly, independently of the crack tip velocity. This becomes even more pronounced for increasing R_0/D (decreasing elastic strip width). Compared to the results in [9], these predictions agree well with the trends found for the overall strain hardening - increased strain hardening lowers the shielding ratio. It should be noticed that at high crack tip velocity, the material rate-sensitivity and strain gradient hardening act together in order to lower the toughness as both mechanisms help to elevate the stresses near the tip (see Fig. 4a). On the other hand, the two mechanisms will be competing at low crack tip velocity. For a slowly growing crack, it has been observed that the level of the peak reference stress close to the crack tip is little affected by changes in the rate-sensitivity when omitting gradient effects (independent of the ratio R_0/D), whereas the surrounding field relaxes with increasing strain rate hardening. Moreover, for a slowly growing crack with $L_D > 0$, it is observed that rate-sensitivity slightly lowers the peak reference stress, while a slight elevation of the wake stress field is observed. Thus, generally speaking; for a slowly growing crack (and $m > 0$), the material has time to relax the stress field that surrounds the tip through plastic straining, whereby the material rate-sensitivity serves as to increase the shielding ratio.

Interestingly, strain gradient hardening is also found to significantly lower the mean stress near the crack tip, and thereby suppresses the stress triaxiality in the region surrounding the fracture process zone (see Fig. 4b). On the other hand, a much smaller effect is found on the stress component that drives failure by cleavage or atomic separation (here being σ_{22}). In fact, the peak of the σ_{22}-component remains nearly unchanged when altering the dissipative length parameter, independently of the ratio R_0/D.

As discussed in [9], the monotonic increase/decrease of the shielding ratio with rate-sensitivity facilitates a definition of a characteristic velocity, for which the toughness is independent of the material rate-sensitivity. As noted from Fig. 3, the current gradient enhanced model exhibit the same monotonic behavior, independently of the dissipative length parameter, L_D. Thus, it is expected that a similar characteristic velocity exists for the current model. This is confirmed from Fig. 5 showing the shielding ratio as function of the crack tip velocity, $\dot{a}/R_0\dot{\epsilon}_0$, where a characteristic velocity is easily identified as the common intersection point for curves with fixed dissipative length parameter.

Comparing Figs. 3 and 5 to the extensive parametric study presented in [9], the limitations of the gradient enhanced model shine through the choice of material parameters investigated. It is well known that the current visco-plastic model formulation becomes numerically unstable for $m \to 0$. In fact, choosing $m = 0.01$ in Figs. 3–5 provides numerical challenges, and similar numerical difficulties are experienced for this model set-up when considering low strain hardening materials (e.g. $N = 0.1$) when the rate-sensitivity is low, especially for $L_D \to 0$. However, these inaccessible regions of the parameter space can be accessed in terms of the rate-independent response by exploiting the characteristic velocity identified from Fig. 5. As discussed, this intersection point is independent of the material rate-sensitivity, thus consequently it directly brings out the
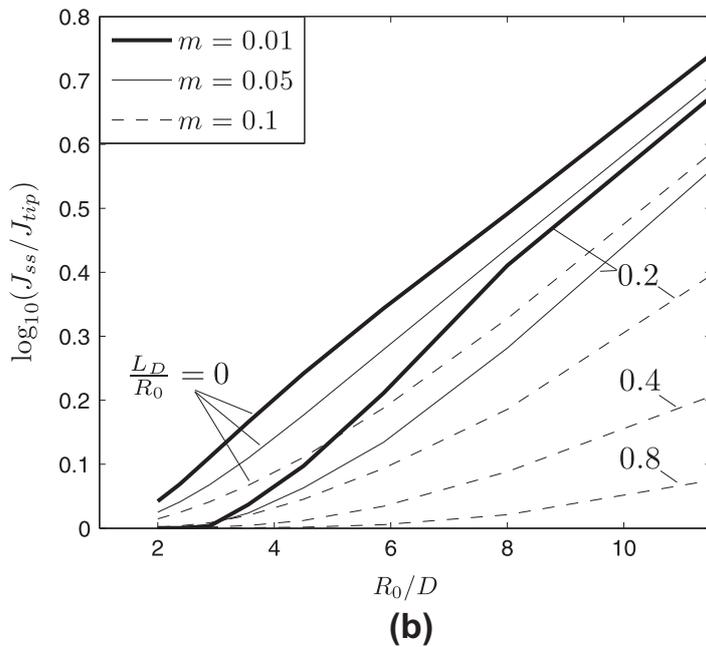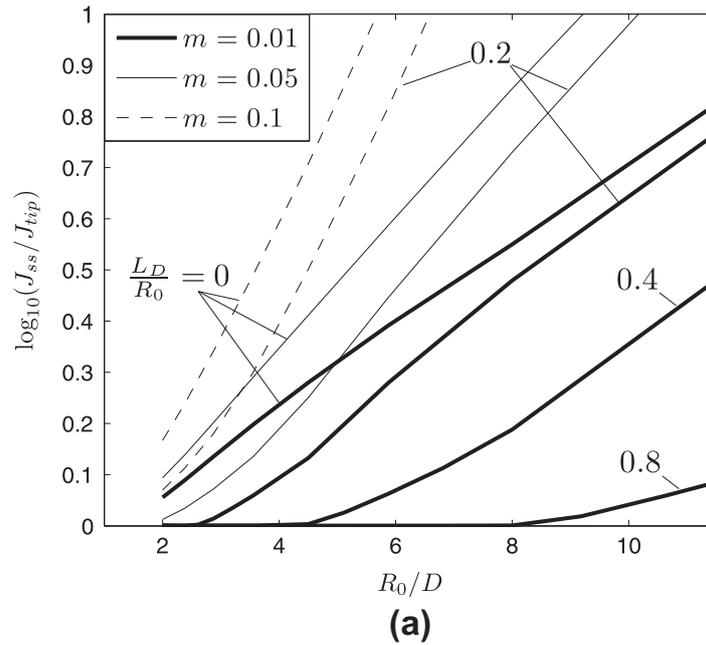
Fig. 3. Steady state fracture toughness vs. inverse elastic layer thickness (SSV parameter "*D*") for a homogeneous material with $N = 0.2$, $m = [0.01, 0.05, 0.1]$, $L_D/R_0 = [0, 0.2, 0.4, 0.8]$, (a) $\dot{a}/(R_0 \dot{\varepsilon}_0) = 10^2$, and (b) $\dot{a}/(R_0 \dot{\varepsilon}_0) = 10^4$.

shielding ratio for the rate-independent limit ($m = 0$ would be a horizontal line in Fig. 5). Moreover, the intersection point has been shown also to exists for high strain rate hardening at which the model is numerically stable - even for low strain hardening and $L_D \rightarrow 0$. Thus, repeated calculations similar to those in Fig. 5, can be used to extract the variation of the rate-independent shielding ratio with a parameter of interest. An example is given in Fig. 6 where each point is extracted from the intersection of two "toughness vs. velocity" curves with $m = 0.1$ and $m = 0.08$, respectively. Results are shown for two levels of strain hardening ($N = [0.1, 0.5]$), and for various values of the dissipative length parameter ($L_D \in [0, 0.4]$). It is seen that the predicted shielding ratio follows the expected trends when compared to Fig. 3 (and to [9]). In addition, the extracted curves for $L_D = 0$ in Fig. 6 is directly compared to the predictions of a corresponding conventional model with an *m*-value that closely resembles the rate-independent limit ($m = 0.001$, see Fig. 6). This comparison is made possible from the choice of higher order boundary conditions as discussed in Section 3.3. From Fig. 6, a remarkably good agreement is obtained for the high strain hardening material ($N = 0.5$), while a somewhat less impressive, but still rather accurate, prediction is obtain for the low strain hardening material ($N = 0.1$). In the case of high strain hardening ($N = 0.5$) convergence is more easily obtained compared to the case of $N = 0.1$ (keeping m and L_D fixed), which are reflected in the accuracy of the predicted shielding ratio. The

(a)

(b)
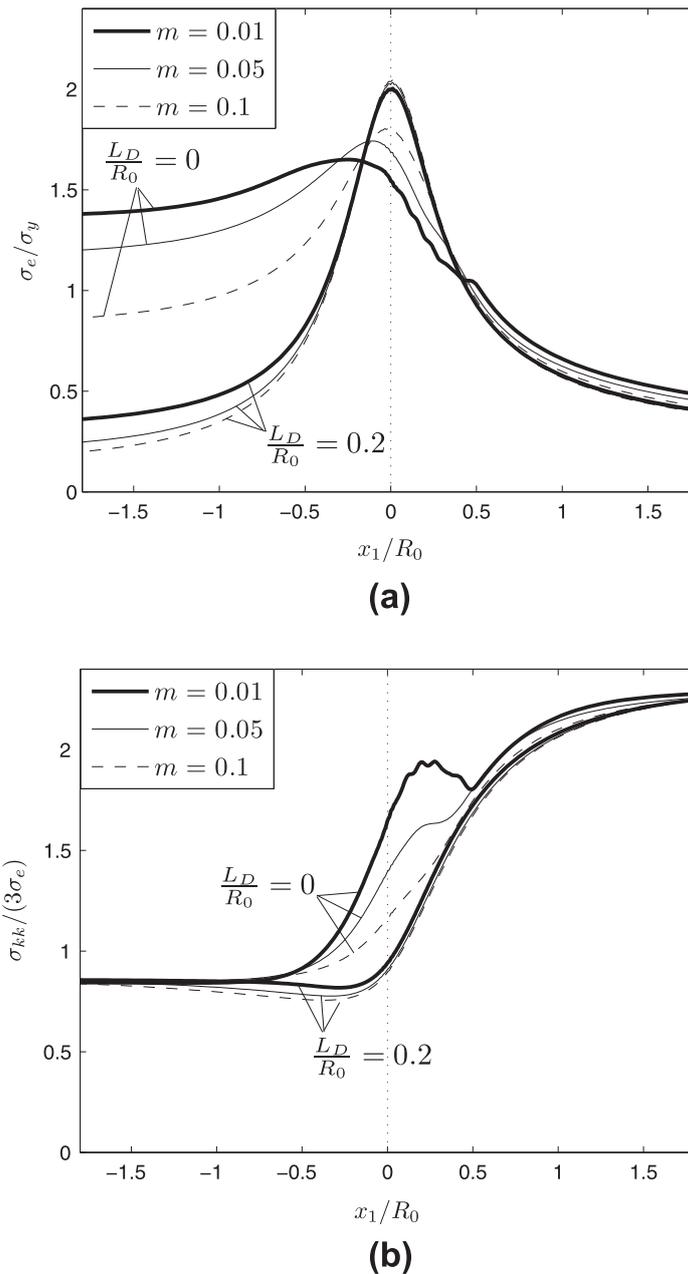
Fig. 4. Variation of (a) von Mises reference stress, and (b) stress triaxiality ($T = \sigma_{kk}/(3\sigma_e)$) along the streamline closest to the SSV-region ($x_2 \approx D$). Here, shown for a fast growing crack ($\dot{a}/(R_0\dot{\varepsilon}_0) = 10^4$) in a homogeneous material with $N = 0.2$, $m = [0.01, 0.05, 0.1]$, $L_D/R_0 = [0, 0.2]$, and $R_0/D = 3.55$.

convergence of the strain gradient dependent model is, however, improved for high values of N, m and L_D. Thus, choosing higher m-values for the intersecting "toughness vs. velocity" curves when considering $N = 0.1$ could improve both convergence and accuracy.

It should be emphasized that Fig. 6 represents the rate-independent toughness which cannot be predicted directly using the current strain gradient model formulation, since the rate-independent theory is incomplete at present. Most importantly issues concerning loading/unloading are yet to be fully resolved (see [36] for further details).

5. Concluding remarks

Mode I toughness of homogeneous strain gradient enhanced visco-plastic metals is studied using a variation of the SSV model with main focus on rate-sensitivity, strain gradient hardening and the possibility of a characteristic velocity, for which the toughness becomes independent of the material rate-sensitivity (see [9] for a further discussion). Questions have been raised whether the characteristic velocity identified in [9] for a conventional model also exists for the current more advanced
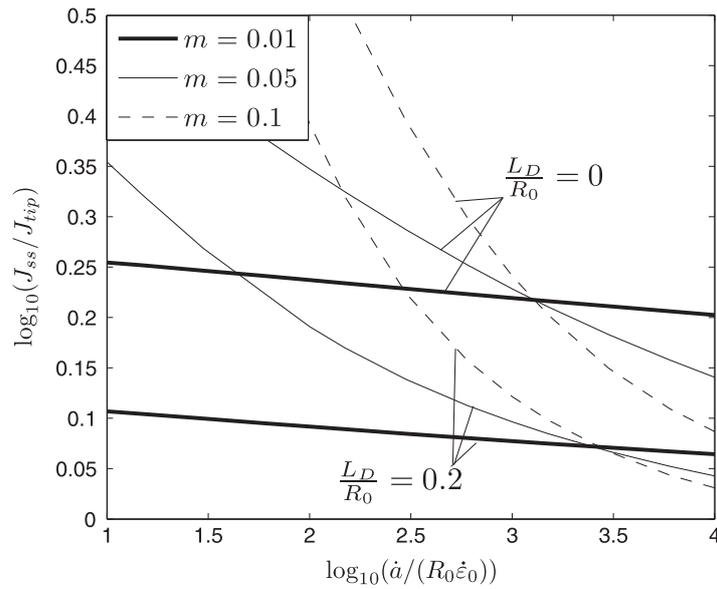
Fig. 5. Steady state fracture toughness vs. crack velocity for a homogeneous material showing the effect of strain gradients for $N = 0.2$, $L_D/R_0 = [0, 0.2]$, $R_0/D = 4$, and $m = [0.01, 0.05, 0.1]$.
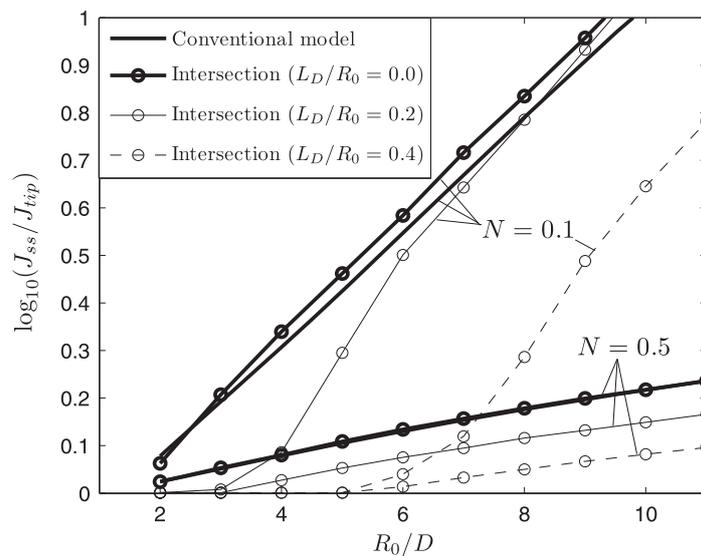
Fig. 6. Steady state fracture toughness vs. inverse elastic layer thickness (SSV parameter "D") for a homogeneous material with $N = [0.1, 0.5]$ and $L_D/R_0 = [0, 0.2, 0.4]$ for $m \to 0$. Here, determined from two intersecting toughness vs. velocity curves with $m = 0.1$ and $m = 0.08$, respectively. The coorsponding conventional results ($m = 0.001$) are shown for comparison.

constitutive model, and if this phenomenon can be exploited in the modeling process. The present work provides a detailed treatment of the steady state modeling procedure for the current model set-up, including a discussion of the choice of higher order boundary conditions. The primary findings for Mode I crack propagation are

- The additional hardening effect owing to strain gradients, that is accounted for through the dissipative length parameter, L_D, lowers the macroscopic toughness for all crack tip velocities considered (see Figs. 3, 5 and 6). This is ascribed to elevated stresses observed near the tip which enable satisfying the fracture criterion at lower macroscopic loads (see Fig. 4).
- Moreover, strain gradient hardening significantly lowers the mean stress near the crack tip, and thereby suppresses stress triaxiality in the region surrounding the fracture process zone (see Fig. 4), whereas a much smaller effect is found on the stress component that drives failure by cleavage or atomic separation.
- The shielding ratio, and thus the macroscopic toughness, displays a monotonic increase with increasing rate-sensitivity at low crack tip velocity, and vice versa at high crack tip velocity (see Fig. 3). This allows for the definition of the characteristic velocity mentioned above (see Fig. 5), which in fact exists for all model settings since the monotonic behavior is found to be independent of all other model parameters.

Despite the lack of physical interpretation of the characteristic velocity, it facilitates a novel approach to model the rate-independent response of metallic materials, characterized by the current visco-plastic model formulation. This approach can be summarized in the following three steps: (i) ensure the monotonic behavior emphasized above, (ii) perform two sets of calculations for different strain rate hardening, m, and plot the parameter of interest (here being the shielding ratio) vs. the crack tip velocity, (iii) identify the intersection point of the two curves, which directly brings out the rate-independent response. An example is given in Fig. 6 for the current steady state model; however, the procedure is believed to apply to a much wider range of problems.

Acknowledgement

References

[1] Dean RH, Hutchinson JW. Quasi-static steady crack growth in small-scale yielding. In: Fracture mechanics: twelfth conference, ASTM STP700. American Society for Testing and Materials; 1980. p. 383–405.
[2] Hui CY. Steady-state crack growth in elastic power-law creeping materials. In: Elastic–plastic fracture: second symposium. Inelastic crack analysis, ASTM STP 803, vol. 1. American Society for Testing and Materials; 1983. p. 573–93.
[3] Suo Z, Shih CF, Varias AG. A theory for cleavage cracking in the presence of plastic flow. Acta Metall Mater 1993;41:1551–7.
[4] Dhirendra VK, Narasimhan R. Mixed-mode steady-state crack growth in elastic–plastic solids. Engng Fract Mech 1998;59:543–59.
[5] Wei Y, Hutchinson JW. Models of interface separation accompanied by plastic dissipation at multiple scales. Int J Fract 1999;95:1–17.
[6] Tvergaard V. Cleavage crack growth resistance due to plastic flow around a near-tip dislocation-free region. J Mech Phys Solids 1997;45:1007–23.
[7] Tvergaard V. Effect of plasticity on cleavage crack growth resistance at an interface. J Mech Phys Solids 1999;47:1095–112.
[8] Tvergaard V. Resistance curves for mixed mode interface crack growth between dissimilar elastic–plastic solids. J Mech Phys Solids 2001;49:2689–703.
[9] Nielsen KL, Niordson CF. Rate sensitivity of mixed mode interface toughness of dissimilar metallic materials. Int. J. Solids Struct. 2012;49:576–83.
[10] Parks DM, Lam PS, McMeeking RM. Some effects of inelastic constitutive models on crack tip fields in steady quasistatic growth. Advances in fracture research. In: Francois D editor. Fifth international conference on fracture, Cannes, France, vol. 5; 1981. p. 2607.
[11] Lam PS, McMeeking RM. Analyses of steady quasistatic crack growth in plane strain tension in elastic–plastic materials with non-isotropic hardening. J Mech Phys Solids 1984;32:395–414.
[12] Niordson CF. Analysis of steady-state ductile crack growth along a laser weld. Int J Fract 2001;111:53–69.
[13] Tvergaard V, Hutchinson JW. The relation between crack growth resistance and fracture process parameters in elastic–plastic solids. J Mech Phys Solids 1992;40:1377–97.
[14] Ma Q, Clarke DR. Size dependent hardness of silver single crystals. J Mater Res 1995;10:853–63.
[15] Stolken JS, Evans AG. A microbend test method for measuring the plasticity length scale. Acta Mater 1998;46:5109–15.
[16] Haque MA, Saif MTA. Strain gradient effect in nanoscale thin films. Acta Mater 2003;51:3053–61.
[17] Swadener JG, George EP, Pharr GM. A microbend test method for measuring the plasticity length scale. J Mech Phys Solids 2002;50:681–94.
[18] Fleck NA, Hutchinson JW. Strain gradient plasticity. In: Hutchinson JW, Wu TY, editors. Advances in applied mechanics, vol. 33. New York: Academic Press; 1997. p. 295–361.
[19] Fleck NA, Hutchinson JW. A reformulation of strain gradient plasticity. J Mech Phys Solids 2001;51:2057–83.
[20] Gudmundson P. A unified treatment of strain gradient plasticity. J Mech Phys Solids 2004;52:1379–406.
[21] Gurtin ME, Anand L. A theory of strain-gradient plasticity for isotropic, plastically irrotational materials. Part I: small deformations. J Mech Phys Solids 2005;53:1624–49.
[22] Lele SP, Anand L. A small-deformation strain-gradient theory for isotropic viscoplastic materials. Phil Mag 2008;88:3655–89.
[23] Gao H, Huang Y, Nix WD, Hutchinson JW. Mechanism-based strain gradient plasticity – I: analysis. J Mech Phys Solids 1999;47:1239–63.
[24] Gurtin ME. A gradient theory of single-crystal viscoplasticity that accounts for geometrically necessary dislocations. J Mech Phys Solids 2002;50:5–32.
[25] Huang Y, Gao H, Nix WD, Hutchinson JW. Mechanism-based strain gradient plasticity – II: analysis. J Mech Phys Solids 1999;48:99–128.
[26] Qiu X, Huang Y, Wei Y, Gao H, Hwang KC. The flow theory of mechanism-based strain gradient plasticity. Mech Mater 2003;35:245–58.
[27] Wei Y, Hutchinson JW. Steady-state crack growth and work of fracture for solids characterized by strain gradient plasticity. J Mech Phys Solids 1997;45:1253–73.
[28] Chen JY, Wei Y, Huang Y, Hutchinson JW, Hwang KC. Strain gradient plasticity. Engng Fract Mech 1999;64:625–48.
[29] Jiang H, Huang Y, Zhuang Z, Hwang KC. Fracture in mechanism-based strain gradient plasticity. J Mech Phys Solids 2001;49:979–93.
[30] Chen SH, Wang TC. Interface crack problems with strain gradient effects. Int J Fract 2002;117:25–37.
[31] Wei Y, Qiu X, Hwang KC. Steady-state crack growth and fracture work based on the theory of mechanism-based strain gradient plasticity. Engng Fract Mech 2004;71:107–25.
[32] Fleck NA, Willis JR. A mathematical basis for strain-gradient plasticity theory – part II: tensorial plastic multiplier. J Mech Phys Solids 2009;57:1045–57.
[33] Rice JR. Elastic fracture-mechanics concepts for interfacial cracks. J Appl Mech Trans ASME 1988;55:98–103.
[34] Ashby MF. The deformation of plastically non-homogeneous materials. Phil Mag 1970;21:399–424.
[35] Ohno N, Okumara D. Higher-order stress and grain size effects due to self-energy of geometrically necessary dislocations. J Mech Phys Solids 2007;55:1879–98.
[36] Niordson CF, Hutchinson JW. Basic strain gradient plasticity theories with application to constrained film deformation. J Mech Mater Struct 2011;6:395–416.
[37] Landis CM, Pardoen T, Hutchinson JW. Crack velocity dependent toughness in rate dependent materials. Mech Mater 2000;32:663–78.